CEAS COUNCIL OF EUROPEAN AEROSPACE SOCIETIES

Design and aerodynamic analysis of a regional turboprop innovative configuration

Fabrizio Nicolosi
Associate Professor
Department of Industrial Engineering (DII)- University of Naples "Federico II"
Via Claudio 21, 80125 Napoli – ITALY
fabrnico@unina.it

Salvatore Corcione
Post Doc

Pierluigi Della Vecchia
Assistant Professor

Vittorio Trifari
PhD student

Manuela Ruocco
PhD student

Agostino De Marco
Assistant Professor

ABSTRACT

This paper deals with the fundamental results of the first loop of design and aerodynamic analysis of a new regional turboprop concept.
The aircraft has a low wing and two innovative architecture of turboprop engine installed at the horizontal tail tips. It can seat up to 130 passengers with a design range of about 3000km. It is designed to fly at Mach number of about 0.62 at a cruise altitude of 9000m with an efficiency about 18. The required maximum lift coefficients in clean, take-off and landing conditions are 1.6, 2.4 and 3.0 respectively.
Wing sections have been specifically designed to comply with the very challenging requirements in terms of minimum drag (natural laminar flow), maximum clean lift coefficients and compressibility effects. The high lift devices have been designed too. A single fowler flap layout has been considered. To augment the aircraft maximum lift capabilities in landing condition, preserving the wing laminar flow, the effects of a simple droop nose have been investigated. To improve climb performance a specific winglet design has been assessed, results show that a reduction of about 10% of the induced drag during both climb and cruise phase could be achieved.
All the criticalities emerged during the first loop will feed a second design loop to well asses this innovative concept.

KEYWORDS: *Aircraft Design, Aerodynamic analysis, Aircraft performance, Innovative Turboprop*

NOMENCLATURE

ADAS - Aircraft Design and Analysis Software
CFD - Computational Fluid Dynamic
CIRA - Italian Aerospace Research Center
DAF - Design of Aircraft and Flight Technologies research group
DATCOM - USAF Stability and Control (Data Compendium)
FL - Flight Level
FusDes - Fuselage Design Methods
IRON - Innovative turbopROp configuration
ISA - International Standard Atmosphere
JPAD - Java-Based Framework for Aircraft Preliminary Design and Optimization
MLW - Aircraft Maximum Landing Weight

MTOW - Aircraft Maximum Take Off Weight
MZF - Aircraft Zero Fuel Weight
NACA - National Advisory Committee for Aeronautics
OEW - Aircraft Operative Empty Weight
RANS - Raynolds Average Navier Stokes
SFC - Specific Fuel Consumption
TLAR - Top Level Aircraft Requirements
TRL - Technology Readiness Level
UNINA - University of Naples
b_w - Wing span
C - wing section chord
C_d - Airfoil drag coefficient
C_D - Aircraft drag coefficient
C_{Do} - Aircraft parasite drag coefficient
C_{Dw} - Isolated wing drag coefficient
C_L - Aircraft lift coefficient
C_l - airfoil lift coefficient
C_{Leq} - Aircraft lift coefficient in trimmed condition
C_{Lmax} - Aircraft maximum lift coefficient
C_{lmax} - airfoil maximum lift coefficient
C_{Lw} - Isolated wing lift coefficient
C_m - Airfoil pitching moment coefficient
C_r - Wing root chord
C_t - Wing tip chord
E - Aircraft aerodynamic efficiency
eps - local wing section twist angle
e_w - Wing induced drag factor
M - Mach number
Re - Reynolds Number
S_w - Wing area
t/c - local wing section non-dimensional thickness
X_{cg} - Centre of gravity longitudinal position
X_{le} - local wing section leading edge longitudinal position
α^* - local wing section angle of attack at the end of lift curve linear segment
α_{zl} - local wing section zero lift angle of attack
η - non-dimensional wing span
λ - Wing taper ratio
$\Lambda_{c/4}$ - Wing sweep angle at the quarter chord line

1 INTRODUCTION

The Innovative turbopROp configuratioN (IRON) project complies with the European Union topic JTI-CS2-2015-CPW02-REG-01-03 (Green and cost efficient Conceptual Aircraft Design including Innovative Turbo-Propeller Power-plant) as part of the Clean Sky 2 program for Horizon 2020.
The topic leader is Leonardo and several core-partners are involved into the project. CIRA (Italian Aerospace Research Center) is coordinator of IRON project.
The project is focused on the feasibility study of an innovative turboprop regional configuration. The research, addressed to the analysis and design of this innovative regional aircraft will be developed through 3 different loops with increasing level of complexity and fidelity. The project aims to complete the design through numerical simulations and experimental validations will be performed so that at the end of the project a Technology Readiness Level (TRL) 4 will be reached.
The loop 1 analysis started in July 2016 from a baseline configuration provided by Leonardo Company. It is an innovative layout with low wing and engines mounted on the horizontal tail tips. Top Level Aircraft Requirements (TLAR) have been issued by Leonardo Company, which also provided the aircraft maximum takeoff weight and wing area. TLAR are very challenging, requiring a cruise speed of 0.62 Mach number at 9144m (30000 feet), with a moderately high lift coefficient and low drag coefficient to achieve a value of 18 in cruise aerodynamic efficiency, a maximum lift coefficient of 1.6 in clean conditions and 3.0 in landing conditions. Moreover, it is expected that the wing inner airfoils have an 18% relative thickness to allow landing gear to be stored within. Most of the design and analysis tools used in this phase are semi-empirical methods and panel codes, with the possibility to perform few CFD RANS analyses to check the obtained results.
In this paper, a summary of the most significant results obtained during the loop 1 of design is presented. The second section of this paper deals with a brief description of the aircraft layout and TLAR requirements provided by Leonardo Company. The third section is focused on the design and the aerodynamic analysis of the wing sections, highlighting all the efforts encountered during the airfoil design phase to comply with the challenging tasks deriving from the TLAR. The fourth section complies with the two-dimensional design of the high lift system and the prediction of the three-dimensional high lift capabilities of the wing. The fifth section illustrates the method used to build up per aircraft components the complete aircraft drag polar in several conditions. These drag polar have been used to perform both stability and control analysis and performance evaluations. Finally, in section 6 some conclusions are drawn highlighting all the criticalities emerged from the loop 1 activities about this innovative aircraft configuration that will feed the input for the loop 2 of design process.

2 IRON REFERENCE AIRCRAFT AND REQUIREMENTS

The reference aircraft, design requirements and Top-Level Aircraft Requirements (TLAR) were provided by Leonardo Company at the beginning of the loop 1. In section 2.1 mission specification and aerodynamic requirements are summarized, and in section 2.2 the baseline geometric layout and its most significant characteristics are illustrated.

2.1 Mission specification and requirements

Design requirements issued by Leonardo on 15 November 2016 are summarized in Table 3, the aerodynamic target and the aircraft baseline assumptions are summarized in Table 2, while some main external geometric characteristics are summarized in Table 1. A sketch of the aircraft layout is presented in Fig. 1.

Table 1: Aircraft baseline input geometric data

Fuselage	Height/width	3.55 m
	Length	38.04 m
Wing	Planform area	100-110 m^2
	Aspect ratio	12
	Leading edge sweep angle	5°-10°

Table 2: Aerodynamic requirements and preliminary weight calculation

Aerodynamic targets	
Cruise efficiency	18
C_{Lmax} landing	3.0
C_{Lmax} T.O. and approach	2.4
C_{Lmax} clean	1.6
Aircraft baseline assumptions	
OEW	33550 Kg
MTOW	53610 Kg
MZFW	49345 Kg
MLW = 97% MTOW	52000 Kg
Payload	13585 Kg
Fuel (Design range)	6475 Kg
Max Str. Payload	15795 Kg
Climb phase	190 KCAS

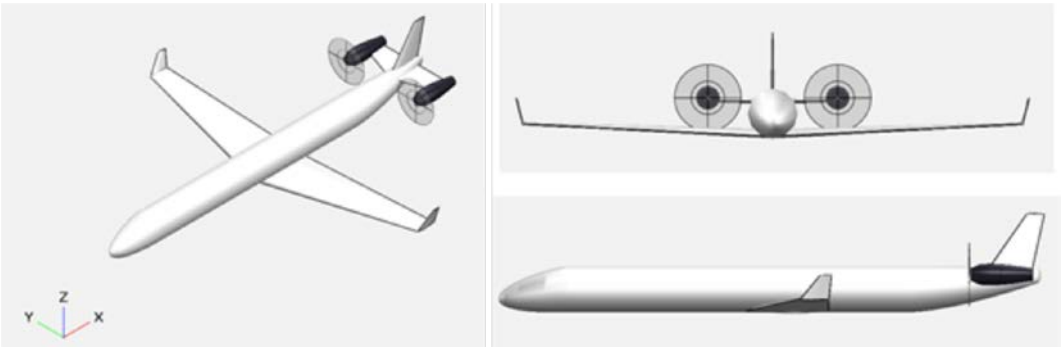

Figure 1: Innovative turboprop aircraft baseline

Table 3: Top Level Aircraft Requirements provided by Leonardo Company

1	**Passenger capacity**	130 pax at 32" seat pitch	
2	**Range with Standard Passenger Payload**	Max payload @ 1600 nm (104.5 Kg x pax); Reserve: a) 30' holding @ 1500 ft b) 100 nm alternate c) 5% of trip fuel	
3	**Cruise Speed**	@ FL300 - ISA - 97% MTOW M_{CR} = 0.62	
4	**Time to climb**	@ MTOW - ISA - from 1500 ft to FL250 <= 13'	
5	**Weight Definition**		
	A	Pax + Baggage	103 Kg @ pax
	B	Catering	1.5 Kg @ pax
	C	OEW	33580 kg
6	**Field Performance**		
	A	Take off field length	ISA - SL -MTOW BFL < 4600 ft (1400m)
	B	Take off from Denver	@ 5400 ft Alt. - ISA+30 - TOW for 400 NM: AC Take-Off with full Pax
	C	Landing field length	@ ISA SL - MLW - Dry runways: LFL < 4260 ft (1300 m)
	D	Steep Approach	Descent approach = 5.5 deg.
7	**CEILING**		
	A	OEI (One Eng. In.)	@ ISA +10° - 97% MTOW - AC ON One Engine Net > 16500 ft (5029 m)

3 AIRFOIL DESIGN AND WING ANALYSIS

To comply with the aerodynamic requirements of the IRON project, a specific airfoil has been designed. The design of the airfoil moved around three main points (see Fig. 2).

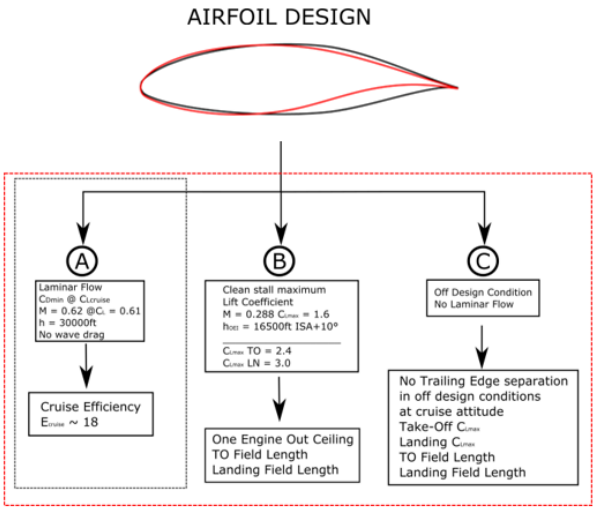

Figure 2: Scheme of the airfoil targets for its design

To match the required cruise efficiency a laminar airfoil (wing) was required, avoiding any drag increase deriving from strong shock waves (Target A of Fig. 2). To reach the prescribed maximum lift coefficients, the airfoil must have a good enough maximum clean lift coefficient (Target B of Fig. 2). Finally, to avoid a large decay of the aerodynamic performance, the off-design conditions must be checked (Target C of Fig. 2). Moreover, Leonardo's requirements provide for a fixed thickness distribution along the wing span: the root and kink sections must have a thickness of 18% of the local chord while the tip section must have a thickness of 14% of the local chord.
To perform the airfoil design, a preliminary wing analysis was required to better understand the most significant aerodynamic conditions at which the airfoil should work. To accomplish this a reference set of airfoil has been assumed. According to the Target A of Fig. 2, a laminar airfoil is needed, thus as good starting points the NACA 66(3)-418 airfoil has been chosen for both root and kink section (having the same percentage thickness), while for the tip airfoil a NACA 63-415, scaled to 14% of thickness, has been considered. These airfoils have been investigated by means of MSES software [1]. The main data to accomplish a preliminary wing analysis are illustrated in Table 4.
The approach used to assess the preliminary wing analysis in terms of lift 3-D lift curve and wing span loading is described in [3]. The wing span loading calculation has been coupled with a classical stall path approach in order to derive the maximum clean lift coefficient of the wing under investigation.
Results of the preliminary wing analysis are shown in Fig. 3, where the wing span loading distribution at a wing lift coefficient of 0.6 is illustrated. The summary of this results is shown in Table 5. This preliminary 3-D analysis allowed to define the aerodynamic conditions for the airfoil design. According to results of Table 5, the wing section should have a minimum drag in the range of lift coefficient of about 0.5 and 0.7 for both root and kink sections, while for the tip the minimum drag should be placed in the range of C_l of about 0.2 and 0.4.

Table 4: main aerodynamic and geometric characteristics of reference set of airfoil and relative aerodynamic conditions

Section	Y(m)	H	C(m)	X_{le}(m)	eps(deg.)	α_{zl}(deg.)	t/c	a*(deg.)	C_{lmax}	CRUISE		STALL	
										Re	M	Re	M
Root	0.00	0.00	4.48	19.09	0.00	-3.21	0.18	12	1.83*	$25.8e^6$	0.620	$17.6e^6$	0.288
Kink	5.32	0.30	3.47	20.00	0.00	-3.14	0.18	12	1.81*	$20.0e^6$	0.620	$13.6e^6$	0.288
Tip	17.75	1.00	1.65	22.22	-2.00	-2.99	0.14	12	1.74*	$9.5e^6$	0.620	$6.5e^6$	0.288

*Estimated with MSES, available experimental data about these airfoil are lower than the numerical estimations [2].

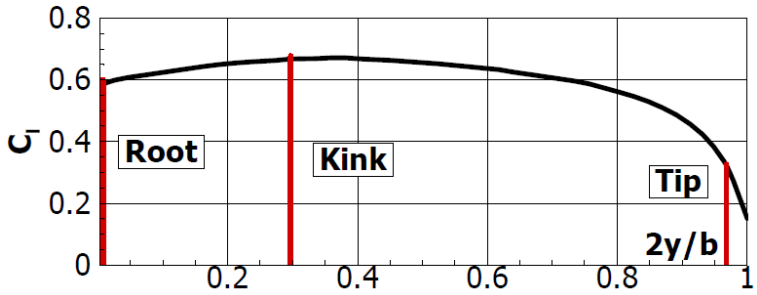

Figure 3: Preliminary 3-D wing span loading at cruise condition (NACA airfoil)

Table 5: Wing sections lift coefficients required to reach a wing C_L = 0.60

Required airfoil lift coefficient for the cruise (wing twist -2°)							
Section	**Y(m)**	**η**	**C(m)**	**X_{le}(m)**	**eps(deg.)**	**t/c**	**C_l cruise**
Root	0.00	0.00	4.48	19.09	0.00	0.18	0.60
Kink	5.325	0.30	3.47	20.00	0.00	0.18	0.68
Tip	17.75	1.00	1.65	22.22	-2.00	0.14	0.25

The design of the airfoil has been accomplished by means of the inverse design routine of MSES software, by modifying the pressure coefficient distribution on the airfoil until the desired aerodynamic characteristics have been reached. The inverse design started from the NACA 66(3)-418 reference airfoil and was focused on the kink airfoil because this is the most significant wing section. The designed airfoil for the kink section is illustrated in Fig. 4, where there is also shown the comparison with the reference NACA airfoil. The main tool used to investigate the aerodynamic characteristics of this airfoil is MSES. Fig. 5 shows the kink airfoil drag polar in cruise condition in both design and off-design (loss of laminar flow, fully turbulent conditions). The minimum drag is spread over a wide range of lift coefficient, the airfoil shows a minimum drag coefficient of about 40 drag counts at the cruise lift coefficient (about 0.6-0.7). This characteristic allows the tip airfoil design can be derived by simply scaling the kink section thickness. Fig. 6 shows the lift curve of the kink airfoil in stall condition. The high lift characteristics have been also assessed by means of numerical analysis performed through a high-fidelity tool like a RANS (Raynolds Average Navier Stokes) solver, as illustrated in Fig. 6 where the comparison between MSES and RANS results is shown. Fig. 7 illustrates the pitching moment coefficient of the kink airfoil in cruise and stall conditions (MSES calculations). Fig. 8 shows the non-dimensional abscissa of the flow transition on the upper and lower surface of the kink airfoil in cruise condition by means of MSES, at cruise condition (Cl around 0.6-0.7 the airfoil exhibits a laminar flow extension of about 50% of the chord). The same numerical analyses have been accomplished also for the root and the tip sections to have a complete airfoil aerodynamic database to be used for the wing analysis.
This airfoil design was not an easy task because of the very challenging aerodynamic requirements and the thickness constraints. This design was a good comprise among the various aspects involved into the design campaign.

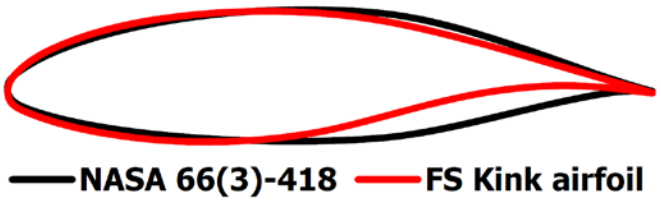

Figure 4: Kink airfoil, comparison with the reference NACA 66(3)-418

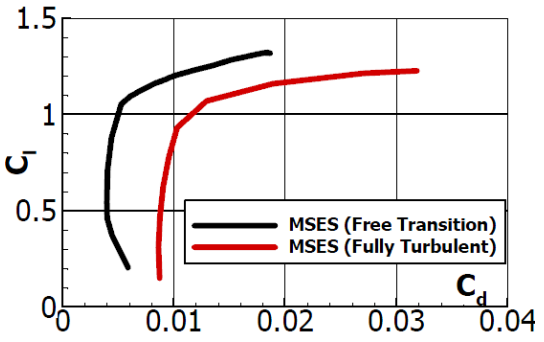

Figure 5: Kink airfoil, drag polar in cruise condition, free transition vs. fully turbulent

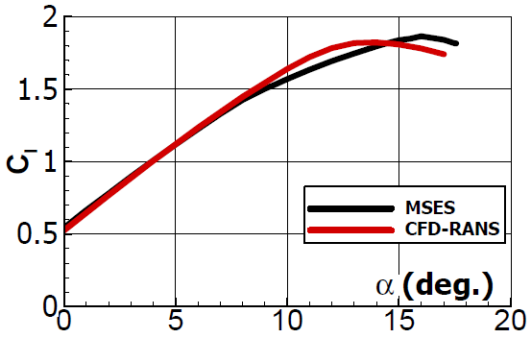

Figure 6: Kink airfoil, lift curve in stall condition, MSES vs. CFD

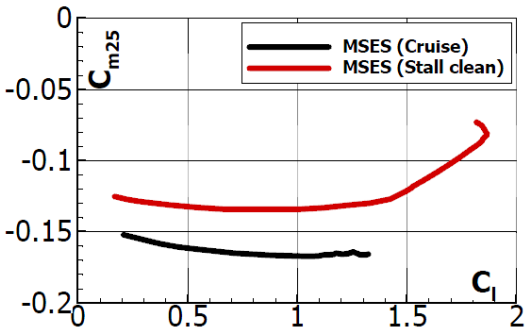

Figure 7: Kink airfoil, pitching moment coefficient in cruise and stall conditions

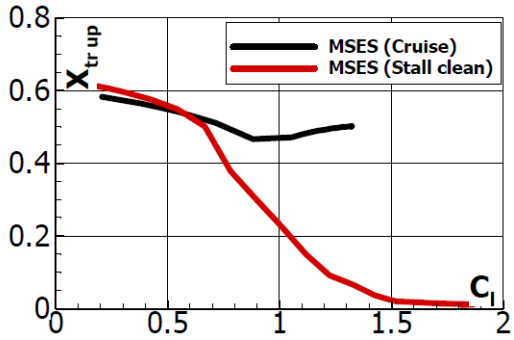

Figure 8: Kink airfoil, non-dimensional transition abscissa

4 2-D HIGH LIFT DEVICES DESIGN AND 3-D WING HIGH LIFT PREDICTION

Once the design of the wing sections has been assessed, the high lift devices design has been accomplished. To meet the requirements provided by Leonardo in terms of maximum lift coefficients for the take-off and landing, a single slot fowler flap has been considered as suitable trailing edge high-lift device. The design of the fowler flap has been assessed for three wing sections: inner flap, kink section and outer flap section. This has been necessary because those three sections have three different flap chord ratios as illustrated in Table 6 and sketched in Fig. 9. Suggestions about the flap chord and wing span extension have been derived from a preliminary design and sizing phase performed at the beginning of the loop 1 of design.

Table 6: Flap geometry and aerodynamic conditions

Sec.	η	c_f/c	Take-Off		Landing	
			M	Re	M	Re
Inner	0.11	0.27	0.171	$16.2e^6$	0.154	$14.5e^6$
Kink	0.30	0.32	0.171	$17.7e^6$	0.154	$16.0e^6$
Outer	0.78	0.32	0.171	$8.8e^6$	0.154	$7.8e^6$

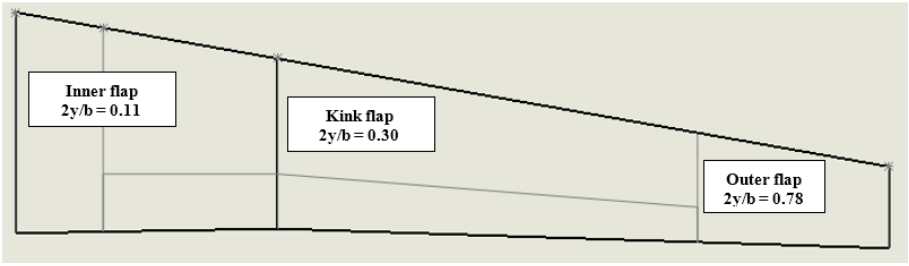

Figure 9: High-lift devices wingspan location sketch

The design of the fowler flap has been performed following the suggestions that can be found in the NASA report CR 2443 [4]. This paper is a report of a two-dimensional wind-tunnel evaluation of two fowler flap configurations on GA(W)-1 airfoil. Two fowler flap configurations are investigated, one configuration has a fowler flap chord of 29% chord and the second one has a flap chord length of 30% of chord. Optimum flap deflection, slot gap and overlap are reported as function of Cl, the maximum achieved C_{Lmax} is 3.8 for a deflection of 40°.
Following the suggestions presented in this report the slot and the flap geometry have been designed on the IRON wing.

Based on the preliminary flap sizing accomplished during the preliminary design phase, where the baseline configuration layout has been assessed by means of two software developed at UNINA called

ADAS (Aircraft Design and Analysis Software) and JPAD (Java-Based Framework for Aircraft Preliminary Design and Optimization) [5][6][7], the high lift systems extends from the 11% to 78% of the wing span and the mean value of the flap chord length is 32% of chord.
The flap design has been performed on the kink section which is the most significant wing section (the 3D wing will exhibit aerodynamic characteristics close to this section), the same flap design parameters derived for the kink have been applied to both inner and outer flap.
The positioning of the fowler flap is achieved by a combined translational and rotational movement that drives the pivot point (see Fig. 10) to be placed in such position that guarantees the best values of both slot gap and slot overlap (these two parameters are defined according to [4]). The pivot point is the centre of the circumference which is tangent to the leading edge of the flap. The deflection angle of the flap is referred to a rigid body rotation around the pivot point.

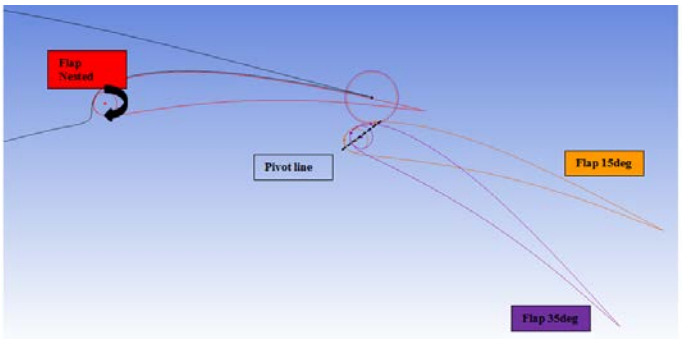

Figure 10: Fowler flap design: flap positioning

To choose the right gap and overlap values different positions of the flap have been analysed by means of MSES tool. The right positioning of the flap has been accomplished by the “airset” routine of MSES software, this routine allows the user to define a reference point (the blue circle in Fig. 11 left) with respect to the flap can be moved and rotated. The right positioning of the flap for a specific deflection has been chosen to place the expansion peak of the pressure coefficient almost at the exit of the flap slot, in order to have the maximum flow acceleration avoiding the flow separation on the flap (see Fig. 11 right). Once the right positioning of the flap has been fixed the flap geometry has been exported in terms of cartesian coordinates and has been analysed by means of both MSES and CFD RANS solver.

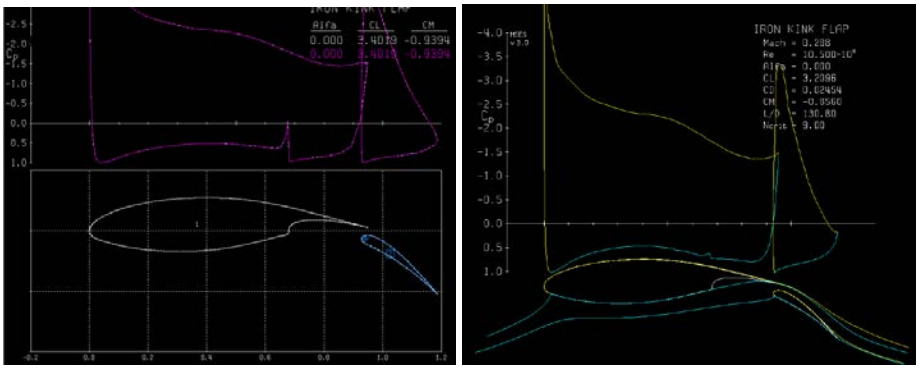

Figure 11: Fowler flap design: flap positioning with “airset” tool of MSES software

Fig. 12 shows the final positions of the kink flap at the three considered flap deflections (15-20° for the take-off conditions and 35° for the landing). Fig. 13 shows the comparison between the numerical results of MSES and CFD-RANS calculations in terms of lift curve for the kink section with a flap

deflection of 15°, while Fig. 14 shows the pressure contour calculated by means of CFD-RANS simulation at the take-off conditions for the kink flap section at angle of attack of 15°.

Same results are shown in Fig. 15 and Fig. 16 where the kink flap section has been analysed at the landing condition with a flap deflection of 35°.

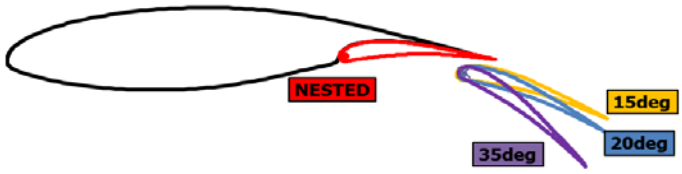

Figure 12: Fowler flap design for the kink section, flap chord length is 0.32% of chord.

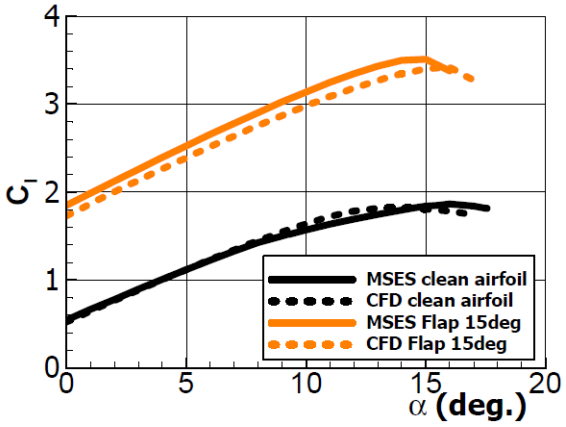

Figure 13: Fowler flap design: flap 15 deg. MSES vs. CFD, M=0.17 Re=13.7e6

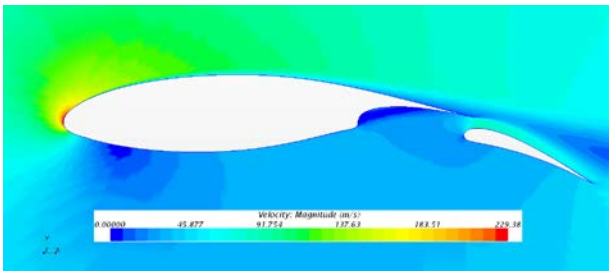

Figure 14: Fowler flap design: flap 15 deg. CFD velocity magnitude contour, M=0.17 Re=13.7e6 alpha = 15°

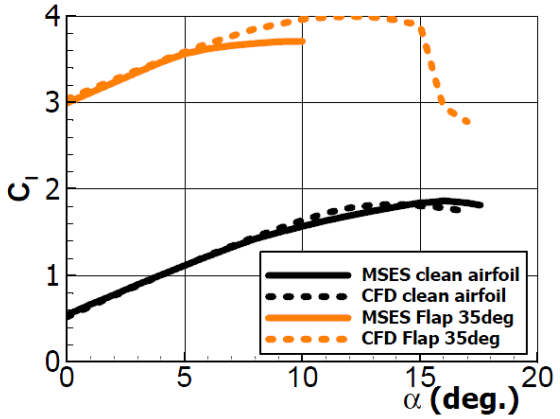

Figure 15: Fowler flap design: flap 35 deg. MSES vs. CFD, M=0.15 Re=12.3e6

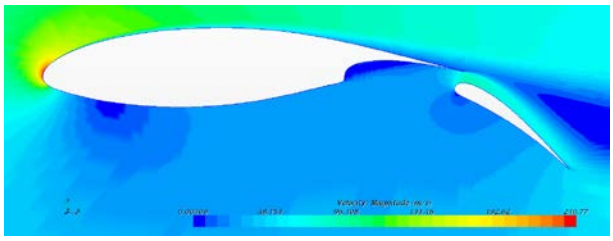

Figure 16: Fowler flap design: flap 35 deg. CFD velocity magnitude contour, M=0.154 Re=12.3e6 alpha = 15°

From Fig. 18 to Fig. 20 the lift curve, the drag polar and the pitching moment variation are illustrated for the kink flap sections at several flap deflections (solid lines).
Table 7 shows the summary of the 2-D results in terms of maximum achievable lift coefficient, ΔC_{lmax} and ΔC_{Do} for the take-off conditions. Same results concerning the landing flap deflection are summarized in Table 8.

Because the prescribed maximum lift coefficients for the landing requirements could be hardly achieved with a single fowler flap, a possible design of leading edge high lift device has been also evaluated. Because the wing laminar flow is mandatory to achieve the target efficiency and the conventional leading edge high lift devices (i.e. slats) disturbs the flow and could cause transition to turbulent flow
immediately after the slat gap, smart seamless and gapless high lift devices at the wing leading edge are mandatory for a laminar wing of significantly increased aerodynamic efficiency.

A possible design of a droop nose here is presented. Authors have investigated the effects of morphing in previous articles [8]. In this case the benefit of the smart droop nose comes from a smooth surface without gaps and steps. Following some suggestions that can be found in the literature [9], a simplified droop nose geometry is here derived and analysed by means of CFD RANS solver, to derive some useful information about the effects of a possible droop nose on the high lift characteristics of the IRON wing.

Table 7: IRON kink flap main results Take Off Conditions Flap=15°, CFD results

Flap 15deg.	C_{lmax}	ΔC_{lmax}	ΔC_l @ α_B=13°	ΔC_d @ α_B=13°	ΔC_m @ α_B=13°
Clean airfoil	1.76	---	---	---	---
Inner section	3.24	1.48	1.24	0.0161	-0.332
Kink section	3.42	1.66	1.45	0.0241	-0.425
Outer section	3.36	1.60	1.31	0.0264	-0.425

Table 8: IRON kink flap main results Landing Conditions Flap=35°, CFD results

Flap 35deg.	C_{lmax}	ΔC_{lmax}	ΔC_l @ α_B=10°	ΔC_d @ α_B=10°	ΔC_m @ α_B=10°
Clean airfoil	1.76	---	---	---	---
Inner section	3.74	2.03	2.16	0.0405	-0.553
Kink section	4.00	2.28	2.46	0.0524	-0.656
Outer section	3.75	2.04	2.26	0.0631	-0.615

The simplest droop nose geometry, here investigated, is obtained by rotating the 15% of the local chord with respect to a point located on the lower airfoil surface at the specified x/c=0.15. This design is a simplification of the droop nose geometry that can be found in [9], where both numerical CFD and experimental wind tunnel tests have been performed to evaluate the effects of droop nose on the high lift characteristics on the airfoil of high efficiency laminar wing. In this preliminary design and analysis of the droop nose, the effects of a deflection of 15 degrees has been considered for all flap conditions. However, in landing conditions the droop nose deflection could be higher than 15°, as suggested in [9], where the best combination was 25 degrees of droop nose with 35-40 degrees of flap. In this work, only the combination of flap 35 degrees and droop nose of 25 degrees has been analysed, useful in landing condition. Fig. 17 shows the simple droop nose geometry used in this analysis.

Figure 17: Kink flap section with 15%c and 15° and 35° of droop nose geometry.

From Fig. 18 to Fig. 20 the effects of the droop nose on the lift, drag and pitching moment coefficient respectively are illustrated concerning the kink section (dotted lines), the same analyses have been performed also on the inner and outer flap sections. The droop nose delays the stall and increases the maximum lift coefficient. In Table 9 and Table 10 the variations in terms of stall angle and maximum achievable lift coefficients are summarized for the take-off and landing conditions

respectively. A droop nose deflection of 15 degrees meanly increases the maximum achievable lift coefficient around 0.1 for each wing section, while a 25 degrees droop nose deflection on 35 degrees of flap increases the C_{lmax} around 0.2. This droop nose design, having an extension of 15% of the chord and a deflection of 15 degrees or 25 degrees, does not affect in a significantly way the pitching moment coefficient.

At high lift coefficients, the droop nose reduces the drag. Comparable results in terms of drag variation can be found in [9]. The drag reduction due to the droop nose can be found at high lift coefficients typical of flap down configurations.

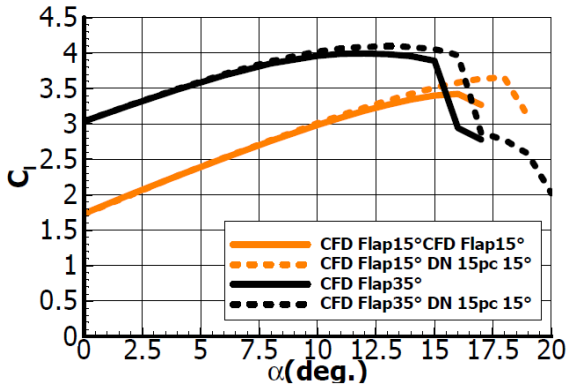

Figure 18: Kink flap section, effect of droop nose on lift coefficient, CFD results

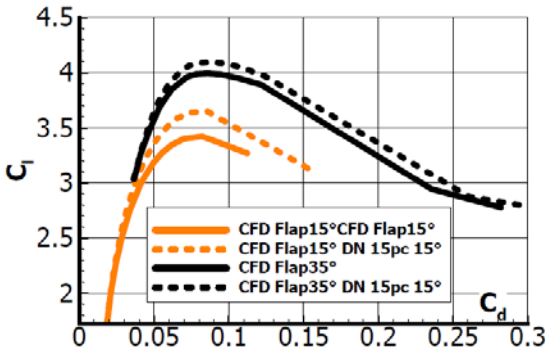

Figure 19: Kink flap section, effect of droop nose on the drag polar, CFD results

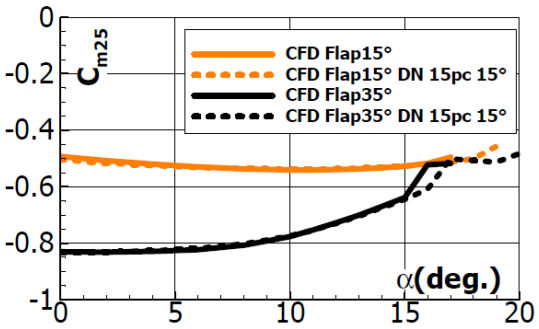

Figure 20: Kink flap section, effect of droop nose on the pitching moment coefficient, CFD results

Table 9: IRON droop nose CFD results Take Off Conditions Flap=15° and Droop-Nose defl. = 15°

	C_{lmax}		ΔC_{lmax} (Droop-Clean)	ΔC_l @ α_B=13° (Droop-Clean)	ΔC_d @ α_B=13° (Droop-Clean)	ΔC_m @ α_B=13° (Droop-Clean)
Clean airfoil	1.76		---	---	---	---
Flap 15deg.	**Flap Only**	**Flap& Droop**				
Inner section	3.24	3.40	1.64	1.35	0.0118	-0.324
Kink section	3.42	3.65	1.89	1.58	0.0181	-0.422
Outer section	3.36	3.57	1.81	1.57	0.0183	-0.400

Table 10: IRON droop nose CFD results Landing Conditions Flap=35°, Droop-Nose defl. =25°

	C_{lmax}		ΔC_{lmax} (Droop-Clean)	ΔC_l @ α_B=10° (Droop-Clean)	ΔC_d @ α_B=10° (Droop-Clean)	ΔC_m @ α_B=10° (Droop-Clean)
Clean airfoil	1.76		---	---	---	---
Flap 35deg.	**Flap**	**Flap&**				

	Only	Droop				
Inner section	3.74	3.99	2.23	2.23	0.0341	-0.557
Kink section	4.00	4.21	2.44	2.56	0.0452	-0.662
Outer section	3.75	4.08	2.32	2.47	0.0452	-0.662

Once the 2-D aerodynamic effects of flap and droop nose have been evaluated, the 3D high lift prediction has been accomplished through semi-empirical approach.

The method here used is a combination of numerical results concerning the 2-D data of the flap sections and a classical semi-empirical approach for the prediction of the 3-D wing high lift characteristics.
Concerning trailing edge devices, the DATCOM method has been used to compute the increment in maximum lift coefficient for the wing [10]. The two-dimensional ΔC_{lmax} have been assumed from the CFD calculations shown in Table 9 and Table 10. According with the 2D C_{lmax} estimation from the CFD calculations, the maximum achievable 3D C_{Lmax} (in untrimmed conditions) are summarized in Table 11. The maximum achievable untrimmed C_{Lmax} is about 2.7 at take-off flap at 15° without droop nose and about 2.8 at flap deflection of 20° without droop nose. In landing configuration with a flap deflected at 40° the C_{Lmax} is about 3.0 without the droop nose and about 3.1 with a droop nose deflected at 25°. To assess the prediction of the maximum lift coefficient of the wing, some CFD-RANS calculations of the isolated wing with flap deflected (without droop nose deflection) have been performed. Results are shown in Fig. 21 and Fig. 22 in terms of lift curve, where the comparison between the semi-empirical 3-D prediction (orange circles) and CFD results (blue circles) is made, some pressure contours and streamlines are shown in Fig. 22 and Fig. 24. The CFD predictions lead to a C_{Lmax} at take-off (flap 15° no droop nose) of about 2.7 at a higher angle of attack than the semi-empirical predictions. At landing the CFD numerical prediction show a C_{Lmax} of about 3.4 larger than the predicted one by means of semi-empirical estimation.

Table 11: High lift devices: aerodynamic coefficient increments in take-off and landing conditions

	ΔC_{Lmax}				ΔC_D				ΔC_M		
Flap	**Flap Only**	**Flap Droop 15°**	**Flap Droop 25°**		**Flap Only**	**Flap Droop 15°**	**Flap Droop 25°**		**Flap Only**	**Flap Droop 15°**	**Flap Droop 25°**
15°	1.04	1.18	---		0.0164	0.0120	---		-0.288	-0.285	---
20°	1.18	1.30	---		0.0219	0.0171	---		-0.341	-0.331	---
35°	1.38	1.45	1.53		0.0373	0.0325	0.0304		-0.443	-0.450	-0.454

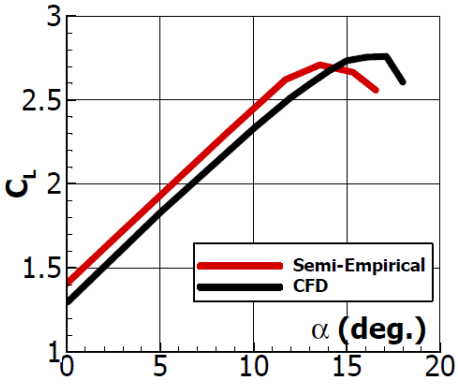

Figure 21: Isolated Wing flap at 15°, CFD vs. Semi-empirical prediction

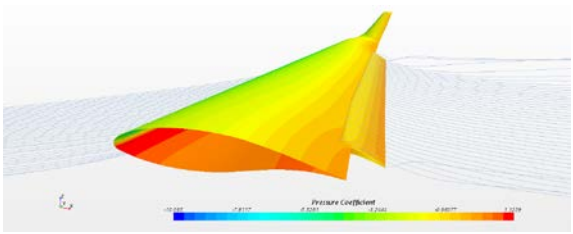

Figure 22: Isolated Wing at take-off conditions with flap at 15°, alpha = 10°

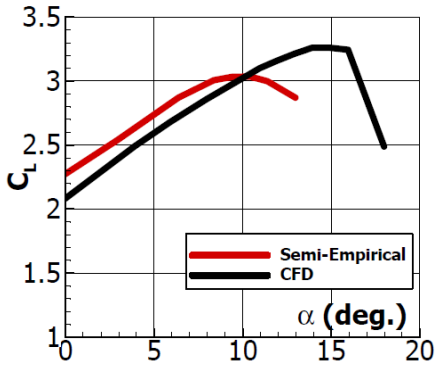

Figure 23: Isolated Wing flap at 35°, CFD vs. Semi-empirical prediction

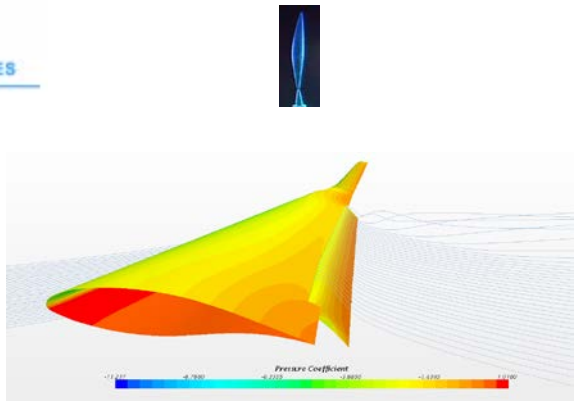

Figure 24: Isolated Wing at landing conditions with flap at 35°, alpha = 10°

5 DRAG POLAR ESTIMATION

Once the aerodynamic design and analysis phase has been accomplished the complete aircraft drag polar has been calculated in several aircraft configurations and conditions (according to the distinct phases of the aircraft mission profile). The fuselage aerodynamic contributions, also in terms of pitching moment instability (which influences the trim drag) has been carefully considered. Several calculations (CFD analysis) have been also performed on the fuselage and classical semi-empirical methods have been applied (see [9-11]). The fuselage results obtained through a dedicated methodology proposed by the authors has been also considered [12].
Several articles, also produced by the authors in the last years, have been used in order to assess the aircraft design and sizing (see [15-17]) and the aircraft drag polar and the aerodynamic contribution of different aircraft components (see [18][19]).
Methods to predict some drag contributions (like fuselage windshield drag) from classical sources (see [20][21]) have been also used. The aircraft drag polar is sum of several contributions calculated as follows:

- **WING**: integration of airfoils drag coefficient (coming from MSES aerodynamic calculations) along the wing span to estimate the parasite contribution. For take-off and landing conditions, the effect of high lift devices has been considered.
- **FUSELAGE**: CFD Navier-Stokes calculations have been used as function of fuselage angle of attack [$C_D=f(\alpha_B)$].
- **HORIZONTAL**: this contribution has been computed in the same manner of wing (integration of airfoil parasite drag along tail span); the drag dependent from horizontal tail lift has also been considered according parabolic formulation with $e_H=0.9$; the drag contribution to trim the aircraft has been calculated as sum of 2 terms: i) $\Delta C_{DTRIM}=f(\Delta C_{LH})$; ii) parasite drag variation due to tail attitude and elevator deflection
- **OTHER COMPONENTS**: Vertical tail, nacelles, wing-fuselage interference, horizontal-nacelles interference, excrescences and miscellaneous items have been considered as a constant parasite drag source (see [20] [21]).
- **TAKE-OFF AND LANDING**: landing gear contribution has been considered according to [20]. In these conditions, only the flap deflections effects have been considered (no droop nose effects have been considered).

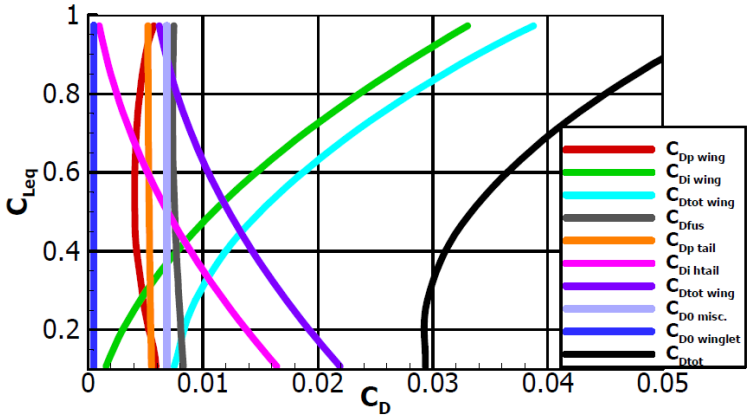

Figure 25: Drag breakdown, Cruise condition at X_{cg} = 0.25 % MAC

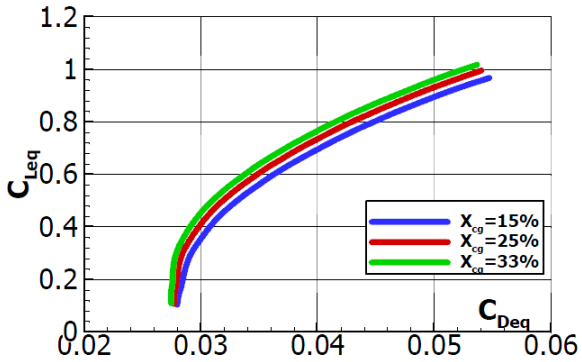

Figure 26: Aircraft trimmed drag polar, Cruise condition at several X_{cg} position

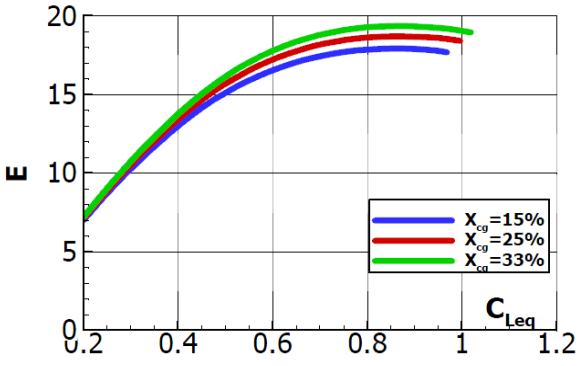

Figure 27: Aircraft efficiency in Cruise, trimmed conditions at several X_{cg} position

Fig. 25 shows the drag breakdown of complete aircraft vs. the trimmed lift coefficient in cruise conditions with a centre of gravity located at 25% of the mean aerodynamic chord of the wing. Fig. 26 shows the trimmed drag polar at several aircraft centre of gravity locations, Fig. 27 shows instead the complete aircraft efficiency. The cruise efficiency is strongly affected by the centre of gravity location and the target of 18 can be achieved only in the most backword position (33% of mean aerodynamic chord). This is due to the high trim drag required for this configuration with rear engine installation.

Fig. 28 shows the comparison between the aircraft efficiency in cruise with and without the winglet with a centre of gravity placed at 25% of MAC. To account for the additional wetted area of the winglet, a ΔC_{D_0} about 5drag counts has been considered. As it can be appreciated the aircraft efficiency in winglet off configuration is always lower than 18. The winglet has been specifically designed for this aircraft giving a reduction of about 10% of the induced drag, especially in the climb condition, but also in cruise, the designed winglet gives a benefit in terms of induced drag reduction since the aircraft will fly at moderately high cruise lift coefficient (about 0.6).

Fig. 29 shows the complete aircraft trimmed drag polar in several conditions with the centre of gravity placed at 25% of the mean aerodynamic chord. Fig. 30 shows the complete aircraft efficiency in clean stall conditions (take-off and first segment climb) at several positions of the centre of gravity.

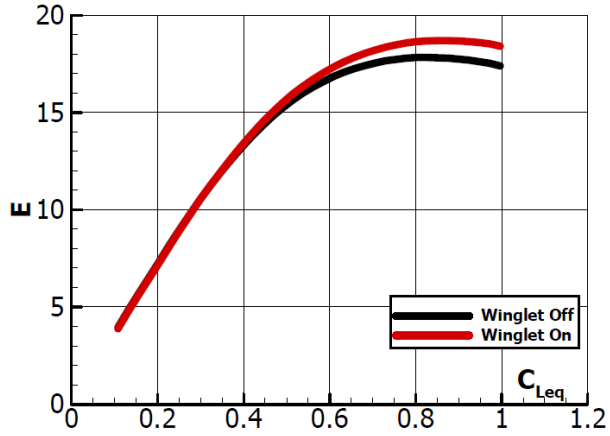

Figure 28: Aircraft efficiency with and without winglet, cruise conditions, at X_{cg}=0.25 % MAC

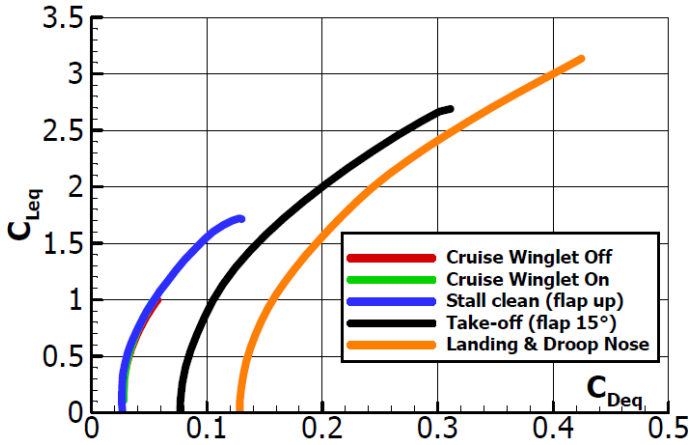

Figure 29: Aircraft trimmed drag polar, for several configurations, X_{cg}=25 % MAC

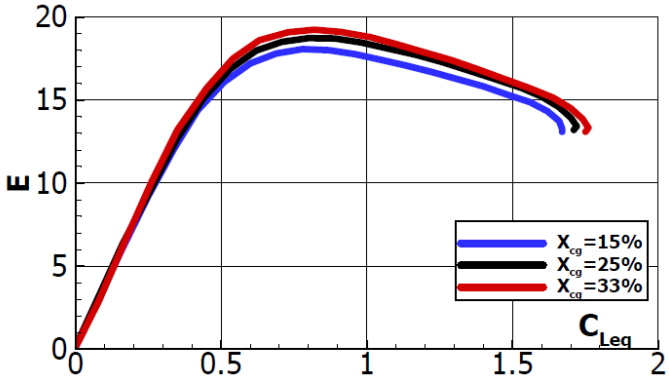

Figure 30: Aircraft aerodynamic efficiency, take-off and first segment climb (flap up) at several X_{cg} positions

6 CONCLUSIONS

The paper presents a synthesis of the main aerodynamic results of the first loop of design of an innovative turboprop aircraft configuration with rear engine installation. A set of wing sections has been specifically designed to comply with the requirements of this project. To reach the prescribed ground performance the high lift devices have been also designed and the effects of a possible morphed droop nose high lift device have been also investigated to augment the maximum lift capability of the aircraft
in take-off and landing conditions.
The complete drag polar breakdown has been performed and the aircraft trimmed drag polar curves have been calculated to produce a complete aerodynamic data set that could feed the evaluation of the aircraft performance (not shown in this paper). Almost all the aerodynamic and performance requirements have been meet, some criticalities dealing with this innovative configuration have emerged. The aircraft efficiency, trim and stability is strongly affected by the center of gravity position. All the criticalities emerged from the first loop of design and analysis will feed a refined assessment of the aircraft layout for a second loop.

AKNOWLEDGEMENTS

The project leading to these results (IRON project) has received funding from the Clean Sky 2 Joint Undertaking under the European Union's Horizon 2020 research and innovation program under *Grant Agreement* n° 699715. The authors are grateful to the partners of the IRON consortium for their contributions and feedback.

REFERENCES

1. M. Drela; 1996;"Two-Dimensional Transonic Aerodynamic Design and Analysis Using the Euler Equations"; *Ph. D. Thesis, MIT.*
2. I.H. Abbott and A.E. Doenhoff; 1949; *Theory of Wing Sections: Including a Summary of Airfoil Data*; Dover Publications, INC; New York.
3. J.A. Jr. Blackwell; 1969; "A finite step method for calculation of theoretical load distribution for arbitrary lifting surface arrangements at subsonic speeds"; *NASA Langley Research Center*; **NASA-TN-D-5335**; Washington, United States; 1st July 1969.
4. W. Seetharam and H.J. Wentz; 1974; "Development of a fowler flap system for high performance general aviation airfoil"; *Center for Research, INC. University of Kansas, Kansas for Langley Research Center;* **NASA CR-2443**; Washington, D.C.; 1st Dec. 1974.
5. F. Nicolosi and G. Paduano; 2011; "Development of A software for Aircraft Preliminary Design and Analysis"; *3rd CEAS Air & Space Conference;* Venezia (IT); 702-714.
6. F. Nicolosi, A. De Marco, L. Attanasio and P. Della Vecchia;2016; "Development of a Java-Based Framework for Aircraft Preliminary Design and Optimization"; *Journal of Aerospace Information System;* **13;** 234-242.
7. V. Trifari, M. Ruocco, V. Cusati, F. Nicolosi, A. De Marco; 2017; "Java framework for parametric aircraft design – ground performance"; *Aircraft Engineering and Aerospace Technology (EMERALD)*; Volume **89**, Issue **4;** DOI 10.1108/AEAT-11-2016-0209.
8. P. Della Vecchia, S. Corcione, R. Pecora, F. Nicolosi, I. Dimino, A. Concilio;2017; "Design and integration sensitivity of a morphing trailing edge on a reference airfoil: The effect on high-altitude long-endurance aircraft performance"; *Journal of Intelligent material system and structures (JIMS)*; ISSN: 1045-389X; DOI: 10.1177/1045389X17704521
9. M. Kintscher, M. Wiedemann and H. Monner; 2011; "Design of a smart leading edge"; *International Journal of Structural Integrity;* **2(4)**; 383-405.
10. P. Sforza; 2014; *Commercial Airplane Design Principles;* Elsevier Science.
11. C. Perkins and R. Hage; 1949; *Airplane Performance Stability and Control*; John Wiley & Sons Inc.
12. F. Nicolosi, P. Della Vecchia, D. Ciliberti and V. Cusati; 2016; "Fuselage aerodynamic prediction methods"; *Aerospace Science and Technology;* 323-343.

13. F. Nicolosi,P. Della Vecchia, D. Ciliberti;2013; "An investigation on vertical tailplane contribution to aircraft sideforce, "; *Aerospace Science and Technology (Elsevier) AESCTE 2873*, Volume **28**, Issue **1**, Pages 401–416; ISSN 1270-9638; DOI: 10.1016/j.ast.2012.12.006.
14. P. Della Vecchia, F. Nicolosi; 2013; "Aerodynamic guidelines in the design and optimization of new regional turboprop aircraft"; *Aerospace Science and Technology (Elsevier) AESCTE*; Volume **38**; Pages 88-104; ISSN 1270-9638; DOI: 10.1016/j.ast.2014.07.018.
15. F. Nicolosi, S. Corcione and P. Della Vecchia; 2016; "Commuter Aircraft Aerodynamic Characteristics through Wind Tunnel Tests"; *Aircraft Engineering and Aerospace Technology (EMERALD)*; Volume **88**; Issue **4**; 4 July 2016; Pages 523-534.
16. F. Nicolosi, P. Della Vecchia and D. Ciliberti; 2015; "Aerodynamic interference issues in aircraft directional control"; *ASCE's Journal of Aerospace Engineering*; Vol. **28**; N. **1**; January 2015, ISSN 0893-1321.
17. F. Nicolosi,P. Della Vecchia and S. Corcione; 2015; "Design and Aerodynamic Analysis of a Twin-engine Commuter Aircraft"; *Aerospace Science and Technology (Elsevier) AESCTE*; Vol. **40**; Jan. 2015; pp. 1-16, ISSN 1270-9638; DOI 10.1016/j.ast.2014.10.008.
18. H. Multopp; 1942; "Aerodynamic of the Fuselage"; National Advisory Committee for Aeronautics; Technical Memorandum 1036.
19. M. Munk; 1924; "The Aerodynamic Forces on Airship Hulls"; National Advisory Committee for Aeronautics; Technical Report 184.
20. J. Roskam; 2000; *Airplane Design – Part VI: Preliminary Calculation of Aerodynamic, Thrust and Power Characteristics.* DAR Corporation; Lawrence (KS).
21. D.P. Raymer; 1999; *Aircraft Design: A conceptual Approach;* 3rd edition; AIAA Education Series.